Improvements of CO_2 Laser Heterodyne Imaging Interferometer for Electron Density Profile Measurements on LHD

Kenji TANAKA, Clive MICHAEL, Leonid VYACHESLAVOV[1)], Andrei SANIN[1)], Kazuo KAWAHATA, Shigeki OKAJIMA[2)], Takeshi AKIYAMA, Tokihiko TOKUZAWA and Yasuhiko ITO

National Institute for Fusion Science, Toki 509-5292, Japan
[1)]*Budker Institute of Nuclear Physics, 630090, Novosibirsk, Russia*
[2)]*Department of Engimeering, Chubu Univertsity, Kasugai 487-8501, Japan*

(Received 7 December 2006 / Accepted 4 June 2007)

After installation of CO_2 laser (wavelength 10.6 μm) heterodyne imaging interferometer (CO_2 HI) in 2001, continuous developments have been carried out to improve the measurements capability and stability of operation. The CO_2 HI works almost without phase jumping at high electron density ($> 1 \times 10^{20}\,m^{-3}$), where the existing far infrared laser (wavelength 118.9 μm) interferometer suffers from fringe jump due to the reduction of signal intensity caused by refraction. However a second interferometer is required to compensate mechanical vibration. A YAG laser (wavelength 1.06 μm) heterodyne imaging interferometer (YAG HI) is presently used for the vibration compensation. In the 10th LHD experimental campaign (2006~2007), sixty four channels of CO_2 HI to measure electron density profile and ten channels of YAG HI to measure mechanical vibration are working. A measurement example of a pellet fuelled high-density discharge is reported.

© *2007 The Japan Society of Plasma Science and Nuclear Fusion Research*

Keywords: LHD, CO_2 laser, interferometer, density profile, least square method, Abel inversion

DOI: 10.1585/pfr.2.S1033

1. Introduction

A heterodyne interferometer is a promising technique to measure the electron density of high temperature plasma because the measurements are based on phase, so it is insensitive to change of laser intensity or detector sensitivity. An interferometer measures the line integrated electron density, so, Abel inversion is necessary to obtain the radial density profile. In order to reconstruct radial profile with good accuracy, it is necessary to have multi channel measurements covering the whole plasma cross section.

In LHD, we installed a multi channel imaging interferometer. Compared with a conventional interferometer using discrete multi beams, in an imaging interferometer, it is easy to have many channels using a multi channel detector array combined with a slab beam. We use of 10.6 μm CO_2 laser for density measurements. A sufficiently powerful (~8 W) and stable laser source is available, and multi channel detector arrays with excellent sensitivity are also available. These can offer good signal to noise ratio for the beating signal for heterodyne detection. However, the phase shift due to mechanical vibration is not negligible, so, we subtract the phase shift due to vibration using a coaxial YAG HI.

Recently improved central particle confinement has been achieved in pellet injected discharges in the high density regime ($> 10^{20}\,m^{-3}$) of LHD [1]. It is strongly required to measure the density profile to understand high density transport physics and plasma control in such a high density region is also required. However, the existing 13 channel 118.9 μm far infrared laser interferometer suffers from fringe jumping at such a high density and many chords fail to measure correctly. This is caused by the reduction of the heterodyne beating signal amplitude when the mixing efficiency gets worse due to the beam bending due to strong density gradient. With the use of a short wavelength CO_2 laser, the fringe jumps due to loss of signal are almost completely avoided, since refraction effects are negligible.

The initial development results are reported in ref [2] and [3]. In this article, additional improvements are reported. Improvements to increase number of channels and stability of operation have been performed.

2. System Description

The transmission and detection optics are shown in Fig. 1 and the beam paths through the plasma are shown in Fig. 2. Two slab beams of the CO_2 and YAG laser are injected, including an edge slab covering the region R = 4.038 ~ 4.282 m, and core slab beam covering the region R = 3.730 ~ 3.963 m,where R is the major radius. And another 30 mm diameter circular beam both CO_2 and YAG laser radiation is injected at R = 3.705 m. This is the local beam for heterodyne detection.

In Fig. 1 (b), the positions of the lenses and curved

author's e-mail: ktanaka@nifs.ac.jp

© 2007 The Japan Society of Plasma Science and Nuclear Fusion Research

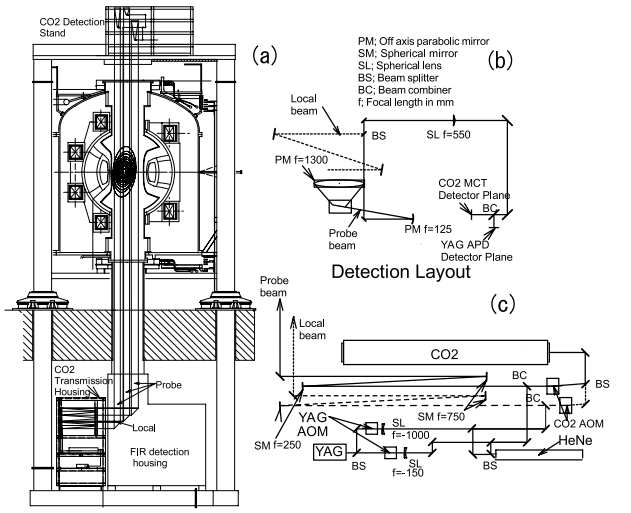

Fig. 1 (a) Schematic view of CO_2 laser interferometer (b) edge beam detection optics and (c) transmission optics.

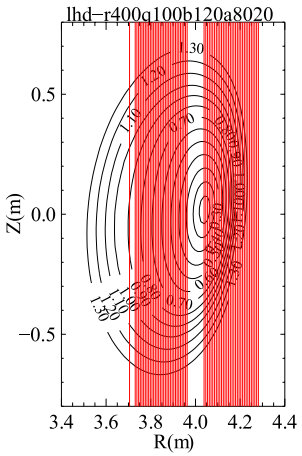

Fig. 2 Measured cross section of CO_2 imaging interferometer. Flux surface is mapped one at $t = 1.2$ sec of Fig. 4 and Fig. 5.

mirrors are determined to have an image of the center of the plasma on the detection plane to minimize spherical aberrations. Two 32 channel detector arrays were used for CO_2 HI, one each for the core and edge beams. The detectors are liquid nitrogen cooled photoconductive type HgCdTe. The chord spacing in the plasma is 7.5 mm in the core beam and 7.9 mm in the edge beam. For vibration compensation, five channels of YAG HI were used for each beam. Slab shaped fiber arrays connected to avalanche photo diodes were used for detection. The replacements to smaller diameter fiber (from 0.5 diameter to 0.1 mm diameter) improved the mixing efficiency making the beating signal of YAG HI more stable. The chord separation of YAG HI is 30~40 mm. In order to compensate the 32 ch CO_2 HI, vibrations were interpolated between YAG HI channels.

The frequency of the CO_2 laser slab beams are shifted by 40 MHz using an acoustic optical modulator (AOM) and the frequency of the CO_2 laser circular beam was shifted 41.01 MHz by another AOM. The CO_2 slab beams and circular beam were mixed on the detection plane and a 10 kHz beating signal was obtained for heterodyne detection. Previously, the beating frequency was 1 MHz, but, from 10^{th} experimental campaign (2006~2007), the beating frequency was reduced down to 10 kHz. This is in order to reduce the cross talk contamination among channels of detector array. This cross talk is due to the voltage drop at the common wiring of the elements. We found that the cross talk is proportional to the signal frequency. Cross talk deforms the measured phase profile especially at edge channels, where the beating signal amplitude is reduced and relative cross talk of the detector is larger. By reducing the beating frequency from 1 MHz down to 10 kHz, crosstalk contamination was reduced by a factor 3~10. The 10 kHz beating signal was sampled at 12.5 kHz. This gives an aliased signal at 2.5 kHz. The phase shifts are calculated by the digital demodulation technique [4].

The 2.5 kHz band width is enough to follow change of the density due to pellet injection, however, sometimes it is not enough to follow rapid change due to radiation collapse and internal collapse by the MHD event. Recent detector developments succeeded to eliminate cross talk contamination connecting each detector elements directly to bias circuit without common wire. This detector is used for two dimensional phase contrast imaging [5, 6]. Also if we replace the presently used current mode amplifier with a voltage mode amplifier, cross talk will be reduced, because the current at the common line becomes smaller and results in a smaller voltage drop on the common line. Also, digital correction of cross talk is possible in principle. We plan to reduce cross talk by the above mentioned technique and to operate at around 500 kHz to have enough bandwidth to follow the rapid change of density and measure fluctuation behavior.

The YAG laser was replaced from 100 mW to 500 mW in order to improve the signal to nose ratio of the YAG heterodyne beating signal. The frequency of YAG slab beam was shifted by 40 MHz and the frequency of YAG circular beam was shifted by 40.99 MHz using two AOMs. The heterodyne beating signal of the YAG laser interferometer was 990 kHz and sampled at 12.5 kHz whose down sampled aliased beating frequency was 2.5 kHz. The phase shifts were obtained using digital demodulation techniques as well as CO_2 HI. In the previous report [3], unstable YAG HI signals were reported. We concluded this is due to the weak laser power and distorted wave front, which caused low mixing efficiency. This causes residual uncompensated vibration components, which is around 1 % of one CO_2 fringe, which corresponds to around $1 \times 10^{18}\,m^{-3}$ of line averaged density. In addition, it was found that instability of laser oscillation caused an unstable YAG signal. The phase signal of YAG HI sometimes drifted and causes vibration compensation to fail. This drifting is likely due to the temporal change of frequency and spatial coherence of

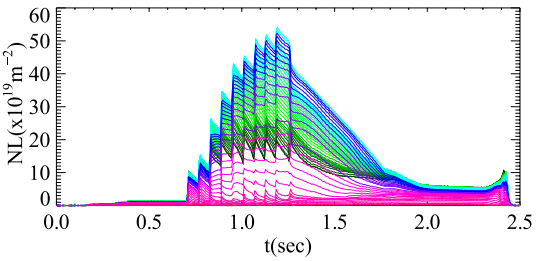

Fig. 3 Example of line density measurements. Mechanical vibration was compensated by YAG laser interferometer.

YAG laser. In order to eliminate phase drifting, the probe and local path length was adjusted to be equal. The position of optics of local beam was adjusted in order to make interference phase output constant sweeping the frequency of the CO_2 laser. We improved the stability of the YAG HI.

The phase shift due to electron density is proportional to laser wavelength and the phase shift due to mechanical vibration is inversely proportional to laser wavelength. The ratio of the contribution of electron density to mechanical vibration of phase shift is proportional to square of laser wavelength. Combination of CO_2 (10.6 μm) YAG (1.06 μm) results in 100 times difference of contribution of electron density, Presently YAG phase shift is subtracted from, CO_2 phase shift. This causes 1 % smaller phase shift, but this is almost comparable with resolution and does not affect reconstruction.

An analog phase counter was also used to provide feedback control of pellet injection timing. An optical link was used to eliminate fringe jumps due to NBI break down noise, which was problem in the previous setup [3].

This system measures phase difference between the channels in the slab beam, however, the edge beam covers the plasma boundary as shown in Fig. 2, so that the absolute phase shift due to plasma density can be measured from the phase difference between the each channel and the channel at the outside of plasma.

3. Experimental Result

Figure 3 is temporal evolution of line density measured by the CO_2 HI with vibration compensation. Abel inversion to obtain radial density profile was done by using linear least square fitting with regularization of the density gradient. These techniques are well established for tomography reconstruction [6]. The inversion was done solving Eq. (2) below for N_e

$$NL_{measured} = (nl_{mes0}, nl_{mes1}....., nl_{mes\,m-1}),$$

$NL_{measured}$; Measured line density, m; chord number

$$N_e = (n_{e0}, n_{e1}, \cdots\cdots n_{en-1}),$$

N_e; rerconstructed local density,
m; number of reconstructed segments

$$NL = A \cdot N_e,\ A;\ \text{Path lenght matrix} \qquad (1)$$

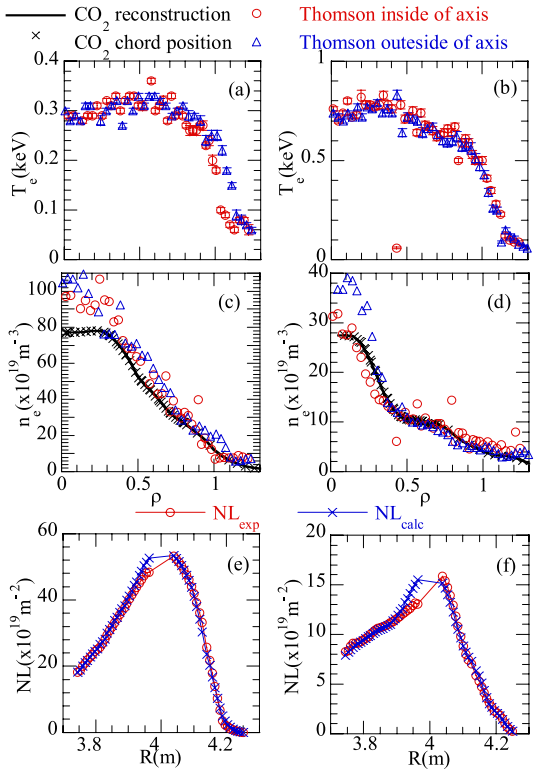

Fig. 4 Measured profiles at around highest central density ((a), (c), (e) t = 1.2 sec) and peaking factor (b), (d), (f) t = 1.7 sec) of the discharge of Fig. 2 (a) (b) Temperature profile from Thomson scattering (c), (d) Comparison of profile by CO_2 HI Thomson scattering. (e), (f) Measure line density and calculated line density of reconstructed density.

W; Weighting matrix,
$w_{i,j} = 1/\sigma^2$ for $i = j$, $w_{i,j} = 0$ for $i \neq j$,
σ is measurments error of NL due to residual vibaration.
D_ρ; Derivative of local density with respect to flux surface coordinate

$$(A^T \cdot W \cdot A + \alpha D_\rho^T \cdot D_\rho) N_e = A^T \cdot W \cdot NL_{measured}$$

α is weighting factor of derivative regulization.

$$N_e = (A^T \cdot W \cdot A + \alpha D_\rho^T \cdot D_\rho)^{-1} A^T \cdot W \cdot NL_{measured} \qquad (2)$$

The regularization parameter α stabilizes the reconstruction to reduce spurious spikes due to noise.

The flux surfaces for the reconstruction procedure were determined as follows. A set of 18 different equilibria were calculated for different beta and pressure profiles with volume averaged beta from 0 % up to 1.2 % with about 0.1 % step. The electron temperature (T_e) profiles help to determine the appropriate equilibrium flux surface. The measurement region of Thomson scattering system covers the whole equatorial plane of horizontally elongated cross section [8]. Then, for each flux surface with different beta, the position in major radius can be converted to the position in flux surface coordinate, which is indicated by

normalized position ρ. Since the data points of Thomson scattering exists inside and outside of magnetic axis, two T_e profiles in the flux surface coordinate $T_e(\rho)$ are obtained for every equilibrium from the database. These two T_e profiles should be identical. Finally, the equilibrium flux surfaces, which minimize the difference between $T_e(\rho)$ from inside and outside of magnetic axis is selected for the reconstruction. Figure 4 (a) and (b) show an example of the result of flux surface selection showing that both inner and outer $T_e(\rho)$ closely match each other.

Figures 4 (c) and (d) show comparisons of the reconstructed density profile and the electron density profile measure by Thomson scattering. The Avalanche Photo Diode (APD) was used for the Thomson scattering and its temperature was controlled constant by water cooling system to keep sensitivity constant. The difference of the sensitivity of APD, the difference of solid angle and scattering volume length of each detection point was taken into account to determine local scattering intensity. So, Thomson raw signal profile should be proportional to electron density profile. Presently, the Thomson signal was not calibrated yet absolutely and relatively from Raman or Rayleigh scattering measurements for calibration. So, the absolute value was determined to match the line integrated value of Thomson signal intensity to the line density measured by microwave interferometer [9], which passed along the same viewing line as the axis of the Thomson scattering system, through at a different toroidal cross section. This calibration factor was obtained shot by shot. Since microwave interferometer suffers from phase jump after pellets are injected, this calibration factor was obtained at low density $(\sim 1\times10^{19}\,\mathrm{m}^{-3})$. Therefore, the YAG laser intensity for Thomson scattering was attenuated to keep linearity of the detector at high density and to use the calibration factor obtained at low density.

Presently, comparison between density profile from Thomson scattering and from CO_2 HI gives rough idea to check validity of two diagnostics. For more precise checking, Thomson calibration experiments are necessary.

As shown in Figs. 4 (c) and (d), the shape of the reconstructed electron density profile and Thomson electron density profiles agree reasonably at $\rho > 0.3$, but a discrepancy can be seen at $\rho < 0.3$. The Thomson electron density profile shows a higher central density.

Figures 4 (e) and (f) show a comparison of the measured line density profile and the line integration of the reconstructed profile. Both agree reasonably in Fig. 4 (e), but a discrepancy can be seen at around $R = 3.9$ m in Fig. 4 (f). The uncompensated vibration components cannot account for this discrepancy. One of the possible reasons is due to the inappropriate flux surface coordinate. The pressure profile, which was used to calculate the equilibrium, is slightly broad one. and is expressed by $P(\rho) = P_0(1-\rho^2)(1-\rho^8)$, where P_0 is central pressure. This pressure profile reasonably agrees with the measure pressure profile at $t = 1.2$ sec, but is much broader than the measured one at $t = 1.7$ sec and causes error of magnetic surfaces.

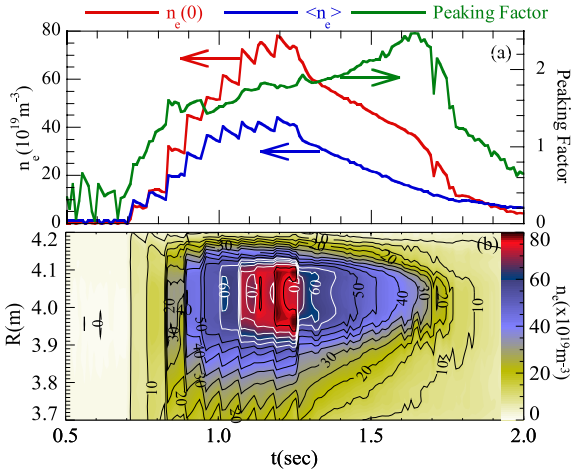

Fig. 5 (a) Temporal evolution of central $n_e(0)$, volume averaged $\langle n_e\rangle$ density and peaking factor $n_e(0)/\langle n_e\rangle$. The volume averaged density was calculated inside of the last closed flux surface. (b) Temporal evolution of radial density profile at the equatorial plane of CO_2 HI cross section.

At $t = 1.2$ sec, the flux surface used for reconstruction is appropriate. So, the discrepancy between CO_2 HI and Thomson scattering might be due to detector saturation effects on the calibration factor of Thomson scattering. At $t = 1.7$ sec, the discrepancy is also due to inappropriate flux surface for reconstruction. The asymmetric inversion procedure, which takes into account of poloidal asymmetry, will help for better reconstruction.

Figure 5 (a) is time history of central and volume averaged density and peaking factor and Figure 5 (b) shows a time history of the reconstructed electron density profile. The central density achieved up to $8\times10^{20}\,\mathrm{m}^{-3}$, and peaking factor achieved around 2.5. The extremely peaking profile was transiently obtained after pellet injection. In Fig. 5 (b), density profile on the equatorial plane of the CO_2 interferometer cross section ($z = 0$ of Fig. 2) are shown. From $t = 0.7$ sec till $t = 1.2$ sec, pellets are injected successively. At $t = 1.25$ sec, which is after the last pellet was injected, density dropped with peaking factor remaining almost constant This drop may be the internal collapse due to the stability limit. After the collapse, the density profile becomes peaked again. This peaking is due to gradually decay of central density and rapid decay of edge density. This suggests difference of particle confinement characteristics between core and edge region.

Acknowledgements

This work was supported by the National Institute for Fusion Science budget NIFS05ULHH511 and Japan Society for the Promotion of Science research funding 1705106

[1] N. Oyabu *et al.*, Phys. Rev. Lett. **97**, 055002-1 (2006).

[2] T. Akiyama *et al.*, Rev. Sci. Instrum. **74**, 1683 (2003).
[3] K. Tanaka *et al.*, Rev. Sci. Instrum. **75**, 3429 (2004).
[4] Y. Jiang *et al.*, Rev. Sci. Instrum. **68**, 902 (1997).
[5] A. Sanin *et al.*, Rev. Sci. Instrum. **75**, 3439 (2004).
[6] C. Michael *et al.*, this proeedings.
[7] M. Anton *et al.*, Plasma Phys. Control. Fusion **38**, 1849 (1996).
[8] K. Narihara, Rev. Sci. Instrum. **72**, 1122 (2001).
[9] K. Kawahata, Rev. Sci. Instrum. **70**, 695 (1999).